

# Hybrid Density Functional Theory Study on the Formation Energies of Donor and Acceptor N Impurities in $\beta$ -Ga<sub>2</sub>O<sub>3</sub>

Asiyeh Shokri,\* Yevgen Melikhov, Yevgen Syryanyy, and Iraida N. Demchenko

Hybrid-density-functional-theory calculations are used to evaluate the structural and electronic properties and formation energies of N-doped  $\beta$ -Ga<sub>2</sub>O<sub>3</sub>. Altogether, eleven interstitial (N<sub>i</sub>) and three substitutional (N<sub>O<sub>I</sub>,II,III</sub>) impurity positions are investigated. Since direct evidence of N<sub>2</sub> formation following the annealing of Ga<sub>2</sub>O<sub>3</sub> and ZnO matrixes is revealed experimentally earlier, four complexes comprising two N atoms are also considered. It is determined that substitutional nitrogen defects act as deep acceptors, whereas the interstitial defects and N<sub>2</sub>-like complexes act as deep donors. Under Ga-rich growth conditions, substitutional nitrogen defects exhibit lower formation energies, with N<sub>O<sub>II</sub></sub> defects being the most favorable. Under Ga-poor conditions, interstitial defects are more energetically desirable for a wide Fermi energy range, with N<sub>i9</sub> defect being the most favorable. The formation of the N<sub>2</sub>-like considered here at solely interstitial positions is energetically very expensive regardless of growth conditions. Finally, the N<sub>i9</sub>-N<sub>O<sub>I</sub></sub> complex is the most desirable one under Ga-rich conditions. This knowledge can serve as a basis for the development of optimal doping strategies, potentially leading to improved performance in future  $\beta$ -Ga<sub>2</sub>O<sub>3</sub>-based electronic devices.

can occur, the monoclinic  $\beta$ -Ga<sub>2</sub>O<sub>3</sub> has excellent chemical and thermal stability, as well as many attractive physical properties. The high bandgap value in the 4.6–4.9 eV range<sup>[1]</sup> leads to a very high breakdown field, theoretically estimated to be 8 MV cm<sup>-1</sup>, much greater than for SiC and GaN.<sup>[2]</sup> In addition, such a high bandgap value would mean less absorption in the ultraviolet. The large Baliga's figure of merit of  $\beta$ -Ga<sub>2</sub>O<sub>3</sub> (3.444) keeps the conduction loss significantly smaller compared to SiC and GaN.<sup>[2–4]</sup> The high saturation electron velocity, theoretically estimated to be around 2 × 10<sup>7</sup> cm s<sup>-1</sup>, is comparable to the values for SiC and GaN but still higher than Si,<sup>[5]</sup> which is desirable for high-frequency applications. Another major advantage is the ability to produce high-quality single crystals cost-effectively using various melt growth techniques.<sup>[5–8]</sup>

One of the recent significant advances concerning this material is the integration of Si and N dopants to engineer a Ga<sub>2</sub>O<sub>3</sub>

## 1. Introduction

The ultrawide-bandgap semiconductor Ga<sub>2</sub>O<sub>3</sub> is a promising candidate to serve as the basis for a new generation of power devices that are smaller and more efficient than the current silicon-based power devices. Among the five crystalline phases in which Ga<sub>2</sub>O<sub>3</sub>


transistor through ion implantation,<sup>[9]</sup> a technique extensively employed in the mass production of commercial semiconductor devices. This advancement is important from the point of view of the ability to introduce two types of impurities (dopants) into the semiconductor, n type and p type, with the aim of developing Ga<sub>2</sub>O<sub>3</sub>-based transistors based on vertical geometry.<sup>[9–11]</sup> Ion implantation aims to either decrease Ohmic contact resistance (shallow donors) and/or to realize potential barriers for voltage blocking (compensating acceptors). Commonly shallow donors applied by ion implantation into  $\beta$ -Ga<sub>2</sub>O<sub>3</sub> include Si, Sn, and Ge,<sup>[12–14]</sup> while compensating acceptors cover Mg and N.<sup>[11,15,16]</sup> Comprehensive research on potential acceptors and donors, coupled with optimization of implantation and thermal annealing processes, is crucial for the eventual realization of practical gallium-oxide-based power electronic devices. To achieve this, it is essential to study how defects and impurities in Ga<sub>2</sub>O<sub>3</sub> affect key material properties. This includes investigating their impact on bandgap, trapping effects, carrier mobility, transition levels, and other properties that are fundamental for future devices.

As is well known, the Ga atoms in  $\beta$ -Ga<sub>2</sub>O<sub>3</sub> occupy two distinct crystallographic sites: tetrahedrally (Ga<sub>I</sub>) and octahedrally (Ga<sub>II</sub>) coordinated. Additionally, there are three unique oxygen sites (O<sub>I</sub>, O<sub>II</sub>, O<sub>III</sub>). All the previously resulted in five possible vacancies or substitutional defect sites. Studies have shown that V<sub>O<sub>III</sub></sub> is the most favorable oxygen vacancy, with lower formation

A. Shokri, Y. Syryanyy, I. N. Demchenko  
Institute of Plasma Physics and Laser Microfusion  
ul. Hery 23, 01-497 Warsaw, Poland  
E-mail: asiyeh.shokri@ifpilm.pl

Y. Melikhov  
Institute of Fundamental Technological Research Polish Academy of Sciences  
ul. Pawinskiego 5b, 02-106 Warsaw, Poland

Y. Syryanyy  
Institute of Microelectronics and Optoelectronics  
Warsaw University of Technology  
ul. Koszykowa 75, 00-662 Warsaw, Poland

 The ORCID identification number(s) for the author(s) of this article can be found under <https://doi.org/10.1002/pssb.202400448>.

© 2024 The Author(s). physica status solidi (b) basic solid state physics published by Wiley-VCH GmbH. This is an open access article under the terms of the Creative Commons Attribution License, which permits use, distribution and reproduction in any medium, provided the original work is properly cited.

DOI: 10.1002/pssb.202400448

energy under O-poor conditions.<sup>[17]</sup> However, all  $V_{\text{O}}$  impurities are deep donors and do not contribute to n-type conductivity. The  $V_{\text{Ga}}$  defect, acting as a deep acceptor, is more likely to form at the  $\text{Ga}_1$  site<sup>[17]</sup> and can cause adjacent Ga atoms to shift to interstitial positions.<sup>[18,19]</sup>

In the present study, we focus on nitrogen dopant since it is considered a potential p-type dopant in  $\text{Ga}_2\text{O}_3$  substituted at the O site, although achieving p-type conductivity remains challenging due to deep acceptor levels introduced by N. When nitrogen substitutes for oxygen, it can act as an acceptor, creating holes (positive charge carriers) in the valence band. Theoretical studies indicate that nitrogen prefers the  $\text{O}_{\text{II}}$  site in a neutral charge state, whereas the  $\text{O}_{\text{III}}$  site is favored for deeper states when the Fermi energy is near the conduction band minimum.<sup>[20]</sup> However, the formation of complexes between N and other native defects, such as O/Ga vacancies, may alter the activation energy required to create free holes, thereby influencing the efficiency of p-type doping. For example, DFT calculations revealed that under Ga-poor conditions (using  $\text{N}_2$  as the dopant source), the  $\epsilon(0/-)$  transition levels for stable  $\text{N}_{\text{O}}-V_{\text{Ga}}$  complexes range from 0.5 to 1 eV, which is markedly lower than the 2.1–3.5 eV transition levels of isolated  $\text{N}_{\text{O}}$  and  $V_{\text{Ga}}$  defects.<sup>[21]</sup> Calculations predict that the spin-polarized state of N-doped  $\beta\text{-Ga}_2\text{O}_3$  is stable, with a magnetic moment of  $\approx 1.0 \mu_{\text{B}}$  per nitrogen dopant, primarily originating from the nitrogen p orbital with minor contributions from surrounding oxygen atoms.<sup>[22]</sup> Previously, it was observed that the introduction of  $\text{N}_2$  molecules into ZnO creates localized states within the bandgap, capturing two holes. This results in reduced effectiveness of p-type doping and significantly affects the electrical properties of ZnO.<sup>[23]</sup> In addition, density-functional theory (DFT) applied for nitrogen-doped ZnO determined the formation energy of various defects and showed an  $\text{N}_2$ -like complex at an O site as the N-related defect with the lowest formation energy.<sup>[24]</sup> Experimental evidence also suggests that similar to ZnO, in  $\beta\text{-Ga}_2\text{O}_3$ , nitrogen may exist as an interstitial molecule or form small  $\text{N}_2$  complexes.<sup>[25]</sup> However, there is still a gap in the detailed study of the preferred defect point for the nitrogen atom in  $\text{Ga}_2\text{O}_3$ , especially interstitial ones. Note that, in theory, under thermodynamically stable conditions, the concentration of N interstitials would be low due to the fact that the formation energy of  $\text{N}_{\text{O}}$  is lower. Nevertheless, one should recall that ion implantation doping is an out-of-equilibrium growth technique that is accompanied by the buildup of a lattice disorder due to the ballistic nature of the process. This would result in various types of defects forming in relatively high concentrations, including, e.g.,  $\text{N}_i$  or  $\text{N}_2$ -like complexes of different kinds.

While most studies have focused on substituting ions and vacancies, the low symmetry of  $\text{Ga}_2\text{O}_3$  offers various sites where inherent and induced impurities can interact, providing opportunities for defect engineering. Blanco et al. provided an insightful, thorough theoretical investigation of point defects in  $\beta\text{-Ga}_2\text{O}_3$ , focusing on ionic conductivity.<sup>[26]</sup> The study, based on the shell model, evaluated the energetics and diffusion characteristics of host lattice and dopant ions, identifying eleven optimal configurations for oxygen and gallium interstitials. Our previous research<sup>[27]</sup> utilized these point defects to study Si interstitials, demonstrating that the Si atom at site i8 is the most favorable interstitial position.

Overall, understanding the exact lattice positions and behavior of dopants is crucial for optimizing annealing processes, which activate dopants after implantation, ensuring they occupy the correct lattice sites to maximize their contribution to conductivity. Moreover, managing the interaction between N dopants and native defects, such as vacancies and interstitials, is essential in large-scale production to maintain consistent device quality and performance. Using DFT, the present study addresses N doping in  $\beta\text{-Ga}_2\text{O}_3$  to investigate defect formation that may impact electronic device operation. Given the limited research on nitrogen interstitials, we focused on exploring these defects by selecting positions reported by Blanco for oxygen atoms, allowing us to identify the optimal interstitial sites for N atoms in  $\beta\text{-Ga}_2\text{O}_3$  based on their formation energy. Additionally, we examined four different pathways of  $\text{N}_2$  formation in  $\beta\text{-Ga}_2\text{O}_3$  to assess the possibility of forming nitrogen  $\text{N}_2$ -like complexes instead of isolated  $\text{N}_i$  interstitials. This understanding would contribute to the knowledge of the optimal doping strategy and, thus, should ultimately lead to enhanced performance in future  $\beta\text{-Ga}_2\text{O}_3$ -based electronic devices.

## 2. Computational Method and Details

First-principles DFT simulations were performed using Vienna Ab initio Simulation Package (VASP, v. 6.3.2) that employs the projector-augmented wave method.<sup>[28–31]</sup> The spin-polarized hybrid DFT was chosen because it is an established approach for studying semiconducting materials that successfully predicts structural, electronic, and optical properties. The Heyd–Scuseria–Ernzerhof (HSE06) hybrid functional<sup>[32]</sup> was employed with the following parameters: the fraction of the Fock exchange was set to  $\alpha = 0.35$ , and a screening parameter was set to  $\mu = 0.20 \text{ \AA}^{-1}$ .

The pristine  $\beta\text{-Ga}_2\text{O}_3$  has a monoclinic crystal structure with space group  $\text{C2/m}$  comprising 20 atoms in the conventional unit cell. The experimental and computed lattice constants are in good agreement,<sup>[22,26]</sup> and for the purpose of this work, the following values are chosen:  $a = 12.23 \text{ \AA}$ ,  $b = 3.04 \text{ \AA}$ , and  $c = 5.80 \text{ \AA}$ . During the optimization of structures, we chose an energy cutoff of 510 eV, force tolerance on each ion was set below  $0.03 \text{ eV \AA}^{-1}$ , and tolerance of total energy was set to less than  $10^{-4} \text{ eV}$  per atom with  $2 \times 8 \times 4$   $\Gamma$ -centered Monkhorst–Pack k-points for a unit cell. For the structures with defects, a  $1 \times 4 \times 2$  supercell of 160 atoms was prepared, and a  $1 \times 1 \times 1$   $\Gamma$ -centered Monkhorst–Pack was used.

The standard procedure to compute the formation energies was utilized as outlined in ref. [27] with the Freysoldt–Neugebauer–Van de Walle correction term to allow the elimination of false electrostatic interactions between charged defect structures.<sup>[33]</sup> The experimental value of the dielectric constant used to calculate this correction term  $E_{\text{corr}}$  was chosen to be 10.<sup>[34]</sup> The defects in charge states of +1, 0, and –1 were considered. In addition to the formation energy curve for a chosen defect, the thermodynamic charge transition level can be identified using<sup>[35]</sup>

$$\epsilon(q_1/q_2) = \frac{E_{q_1}^f|_{E_F=0} - E_{q_2}^f|_{E_F=0}}{q_2 - q_1} \quad (1)$$

where  $E_q^f|_{E_F=0}$  is the formation energy of the structure with the defect in charge state  $q$  evaluated at  $E_F = 0$ . To compute the formation energy, the following values for the chemical potentials of the elements were chosen:  $-11.075$  eV for O (from  $O_2$  molecule) and  $-3.38$  eV for Ga (bulk Ga metal), enabling the determination of the O-rich (Ga-poor) and Ga-rich (O-poor) growth conditions limits. The chemical potential of the N atom is referenced to the  $N_2$  molecule ( $-10.78$  eV) for the Ga-poor condition and to GaN ( $-12.09$  eV) for the Ga-rich condition, analogous to the approach used in ref. [20].

### 3. Results and Discussion

The band structure of pure  $\beta\text{-Ga}_2\text{O}_3$  is shown in **Figure 1**. An indirect bandgap value of  $E_g = 4.91$  eV computed with HSE06 hybrid functional agrees well with the literature,<sup>[27,36]</sup> as opposed to the generalized gradient approximation (GGA) functional calculations that underestimate the bandgap significantly ( $E_g = 2.17$  eV) despite reporting quite similar band structures in the valence and conduction bands. Note that in the literature,  $\beta\text{-Ga}_2\text{O}_3$  can be found to be referred to as either a direct (e.g., ref. [37]) or an indirect (e.g., refs. [38,39]) bandgap semiconductor. The results of our calculations indicate that the indirect transition in  $\beta\text{-Ga}_2\text{O}_3$  is only 0.04 eV lower in energy than the direct transition (4.95 vs 4.91 eV), similar to the value reported in ref. [39]. Consequently, in the case of optical studies, the close proximity of the direct bandgap and its dominance in optical measurements create difficulties in the definitive experimental classification of  $\beta\text{-Ga}_2\text{O}_3$ .

To study the  $\beta\text{-Ga}_2\text{O}_3$  system with N impurity, we considered both the substitutional and interstitial point defects that N can

form in the matrix, as well as some of their complexes. For the substitutional defects, since there are three inequivalent oxygen sites in the crystal structure of  $\beta\text{-Ga}_2\text{O}_3$ , and knowing that N would prefer to substitute O, three substitutional defects were considered:  $N_{\text{OI}}$ ,  $N_{\text{OII}}$ , and  $N_{\text{OIII}}$ . For the interstitial defects, 11 distinct positions, designated  $i_1$  through  $i_{11}$ , were considered based on the topology of the electron density in the low-symmetry structure.<sup>[26]</sup> The positions of the substitutional and interstitial point defects in the  $\beta\text{-Ga}_2\text{O}_3$  matrix are shown in **Figure 2**. Note that these positions represent the initial locations of defects in the perfect  $\beta\text{-Ga}_2\text{O}_3$  matrix before relaxation. After placing a defect at a selected position, a relaxation procedure is performed, allowing atoms to shift. The resulting final configuration was then used to calculate formation energies and other properties. This final configuration might differ substantially from the initial configuration, especially in the case of interstitial defects, similar to Si defects in  $\beta\text{-Ga}_2\text{O}_3$ .<sup>[27]</sup> For example, N atoms initially placed at  $i_7$  and  $i_8$ , after the relaxation procedure, exchanged position with the nearest oxygen atoms  $O_{\text{II}}$  and  $O_{\text{III}}$ , respectively. Nevertheless, we retain the initial notation (e.g.,  $N_{i7}$  and  $N_{\text{OI}}$ ) to describe different cases throughout this study.

**Table 1** summarizes the formation energies and bandgaps for all examined defects in a zero-charge state under Ga-rich and Ga-poor conditions. All substitutional defects have lower formation energies than the interstitial defects, with  $N_{\text{OII}}$  having the lowest formation energy among them, which is in agreement with previous findings.<sup>[20]</sup>

Aiming to analyze the possibility of forming nitrogen molecules in  $\beta\text{-Ga}_2\text{O}_3$ , we selected  $N_{i7}$ ,  $N_{i8}$ , and  $N_{i9}$  as a few interstitial defects for further computational analysis based on their calculated formation energies. The interstitial cases  $N_{i7}$ ,  $N_{i8}$ , and  $N_{i9}$  exhibit distinctively lower formation energies than other

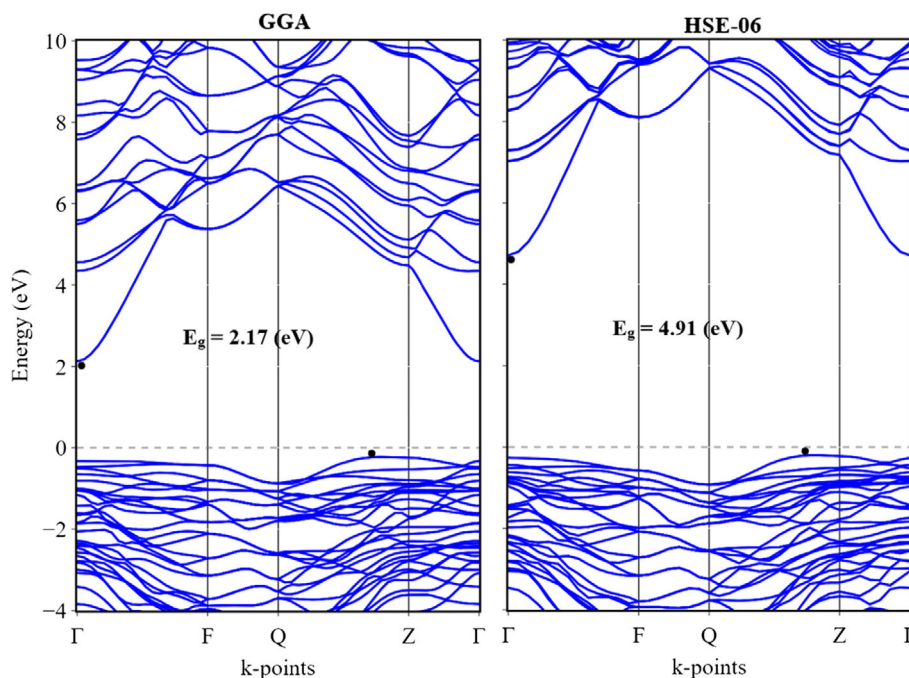


**Figure 1.** Band structure of pure  $\beta\text{-Ga}_2\text{O}_3$  along a continuous path in the Brillouin zone with the high-symmetry points labeled according to ref. [41]. The maximum of the valence band and the minimum of the conduction band are shown with black dots.

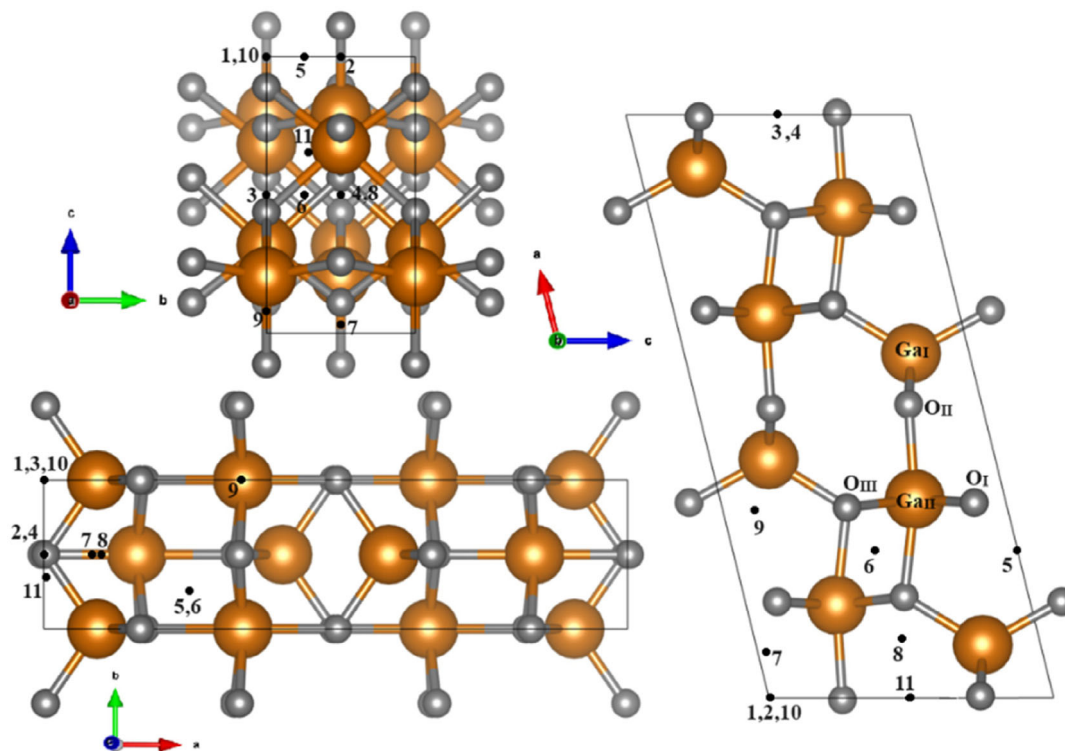


**Figure 2.** Eleven different initial interstitial positions in  $\beta$ -Ga<sub>2</sub>O<sub>3</sub>, views from the top of a) b, b) c, and c) a directions (gold spheres are Ga atoms, and grey spheres are oxygen atoms; interstitial positions are shown with “x” and i).

**Table 1.** Formation energies ( $E^f$ ) in Ga-rich and Ga-poor conditions, and bandgaps ( $E_g$ ) in eV for all defects.

Defect	$E^f$ [eV] (Ga rich)	$E^f$ [eV] (Ga-poor)	$E_g$ [eV]	$E_{Mtot}$ [ $\mu$ B]
N <sub>i1</sub>	9.45	8.14	3.70	–
N <sub>i2</sub>	9.09	7.78	3.35	–
N <sub>i3</sub>	10.40	9.09	3.31	–
N <sub>i4</sub>	8.93	7.62	3.70	–
N <sub>i5</sub>	7.42	6.11	4.29	–
N <sub>i6</sub>	8.96	7.65	4.03	–
N <sub>i7</sub>	6.75	5.44	3.31	1
N <sub>i8</sub>	6.58	5.27	3.89	1
N <sub>i9</sub>	6.86	5.55	2.93	1
N <sub>i10</sub>	7.49	6.18	3.21	–
N <sub>i11</sub>	7.70	6.39	2.95	–
N <sub>i7</sub> –N <sub>OII</sub>	6.84	8.10	2.58	2
N <sub>i8</sub> –N <sub>OIII</sub>	7.11	8.38	2.97	2
N <sub>i9</sub> –N <sub>OI</sub>	5.57	6.84	3.17	2
2N–i7	13.62	11.00	3.41	–
N <sub>OI</sub>	2.47	5.05	4.42	1
N <sub>OII</sub>	2.21	4.79	4.70	1
N <sub>OIII</sub>	3.16	5.74	3.08	1

interstitial cases. The formation energy of N<sub>i5</sub> is higher by 0.57 eV, while for the remaining cases, the difference exceeds 1 eV.

To create a possibility for a nitrogen molecule formation, a second N atom was introduced in each of the relaxed cases N<sub>i7</sub>, N<sub>i8</sub>, and N<sub>i9</sub>. This was done by replacing the O atom nearest to the interstitial N with another N atom, followed by a subsequent relaxation of the structure. These new configurations are designated as N<sub>i7</sub>–N<sub>OII</sub>, N<sub>i8</sub>–N<sub>OIII</sub>, and N<sub>i9</sub>–N<sub>OI</sub>. In addition, owing to the symmetry positions of i7 in the ideal structure, it is possible to place two N atoms in close proximity, both at the i7 equivalent positions, and with a separation of 1.8 Å (note that this cannot be done for the i8 or i9 cases). The subsequent relaxation of this structure, designated as 2N–i7, resulted in slight displacements of neighboring atoms but did not lead to a drastic change in the final configuration, unlike the N<sub>i7</sub> case.

**Figure 3** shows the final positions for N<sub>2</sub> defects and their surroundings for N<sub>i7</sub>–N<sub>OII</sub>, N<sub>i8</sub>–N<sub>OIII</sub>, N<sub>i9</sub>–N<sub>OI</sub>, and 2N–i7. The relaxation procedure resulted in 1.26, 1.31, and 1.27 Å bond lengths between two nitrogen atoms in N<sub>i7</sub>–N<sub>OII</sub>, N<sub>i8</sub>–N<sub>OIII</sub>, and N<sub>i9</sub>–N<sub>OI</sub>, respectively. However, in the case of 2N–i7, the bond length between N atoms is 1.10 Å, which is very close to the value of the bond length in N<sub>2</sub>.<sup>[40]</sup> The electron density distributions shown in **Figure 4** confirm the existence of strong bonds between N atoms in both N<sub>i9</sub>–N<sub>OI</sub> and 2N–i7 cases, with a bond in the 2N–i7 case being stronger. In the N<sub>i9</sub>–N<sub>OI</sub> case, there is an interaction between one of N and Ga, whereas in the 2N–i7 case, the interactions between either N and Ga are weaker. For comparison, the electron density distribution for the N<sub>i8</sub> case, which has the lowest formation energy among isolated N interstitials in a neutral charge state, is also presented in **Figure 4**. In this case, the displacement of the O atom from its

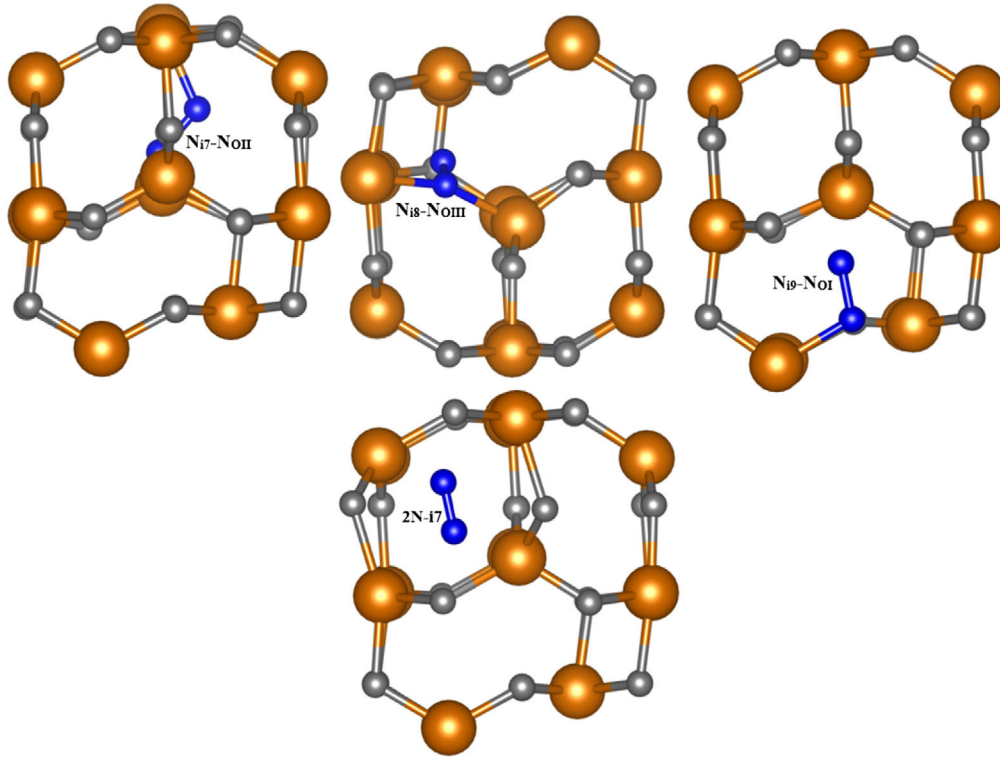


**Figure 3.** Relaxed structure of  $N_2$ -like defects. Gold spheres are Ga atoms, grey spheres are oxygen atoms, and blue spheres correspond to N atoms.

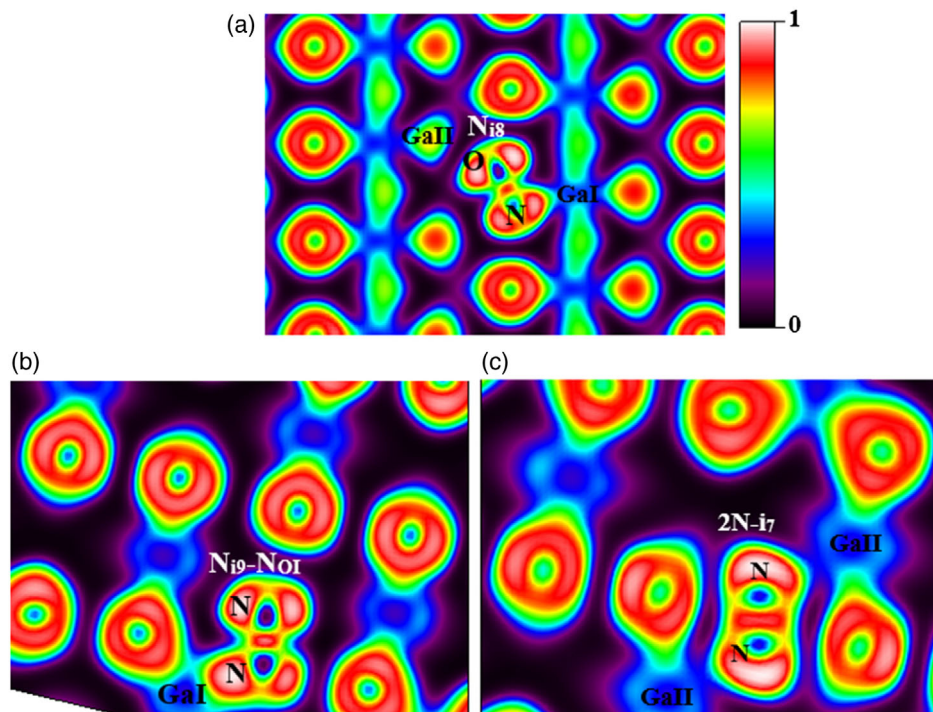


**Figure 4.** The distribution of electron density for a)  $N_{i8}$  in ref. [1] direction, b)  $N_{i9-N_{oi}}$ , and c)  $2N-i7$  in ref. [10] direction.

original position to an interstitial site is visible, resulting in no bond between O and Ga atoms.

Figure 5 presents the density of states for selected defects, taking spin-polarization into account. Notably, some defects induce magnetism in the resultant structure (see also Table 1 for reported total magnetic moments). Previous studies predicted that nitrogen

might introduce stable spin-polarized states in  $\beta\text{-Ga}_2\text{O}_3$ , but only for the substitutional defects.<sup>[22]</sup> However, our choice of a more accurate exchange-correlation potential (hybrid vs GGA) and larger supercell (160 atoms vs 40 atoms) indicates that not only substitutional defects lead to stable spin-polarized states. Instead, interstitial nitrogen and  $\text{N}_2$  complexes contribute a magnetic

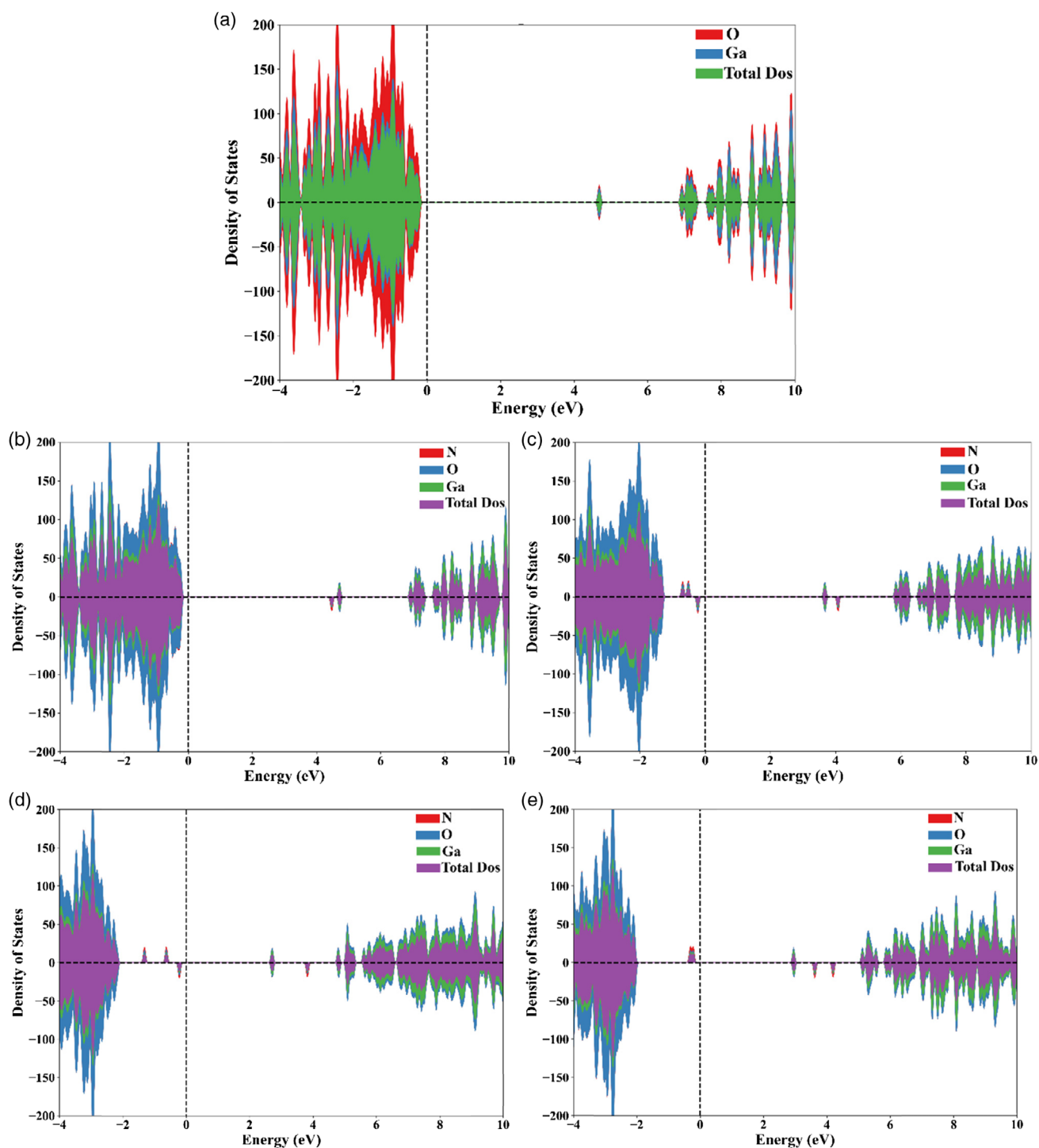


**Figure 5.** Projected density of states for a) pure  $\beta\text{-Ga}_2\text{O}_3$  and for the cases with defects/complexes for 0 charge state: b)  $\text{N}_{\text{OII}}$ , c)  $\text{N}_{\text{I8}}$ , d)  $\text{N}_{\text{I9}}$ , and e)  $\text{N}_{\text{I9}}\text{-N}_{\text{OI}}$ .

moment of  $1.00 \mu_B$  per N atom to the system. The band structure for the same selected defects is shown in **Figure 6**.

**Figure 7** presents the formation energies for the considered cases, taking into account the charge states. Starting with the substitutional defects, it is seen that N substituted at the  $O_{II}$  site has the most favorable formation energy compared to the substitutional positions  $O_I$  and  $O_{III}$ . These defects are also deep acceptors, consistent with earlier findings by Peelaers et al.<sup>[20]</sup> The minor differences observed in the formation energy values can be attributed to variations in computational parameters: energy cutoff (400 vs 510 eV), supercell size (120 atoms vs 160 atoms), and supercell multiplicity ( $3 \times 2 \times 2$  vs  $1 \times 4 \times 2$ ). In the case of interstitial defects  $N_{i7}$ ,  $N_{i8}$ , and  $N_{i9}$ , they are

not favorable compared to substitutional cases over the whole Fermi energy range under Ga-poor conditions. However, under Ga-poor conditions, they become energetically more favorable, at least until  $E_f = 2$  eV. Nevertheless, these defects are deep donors under both growth conditions.

Among the complexes that form  $N_2$ , despite exhibiting the bond length value closest to that of  $N_2$ , the  $2N-i7$  case nevertheless has the highest formation energy among all examined defects (see Table 1). That means that the formation of  $N_2$  at the interstitial position in a matrix of a semiconductor is quite expensive, which is consistent with the results obtained in a similar study by Peelaers et al. for  $N_2$  in the  $\beta$ - $Ga_2O_3$  matrix<sup>[20]</sup> or by Gao et al. for  $N_2$  in ZnO matrix.<sup>[24]</sup> In contrast, under Ga-rich

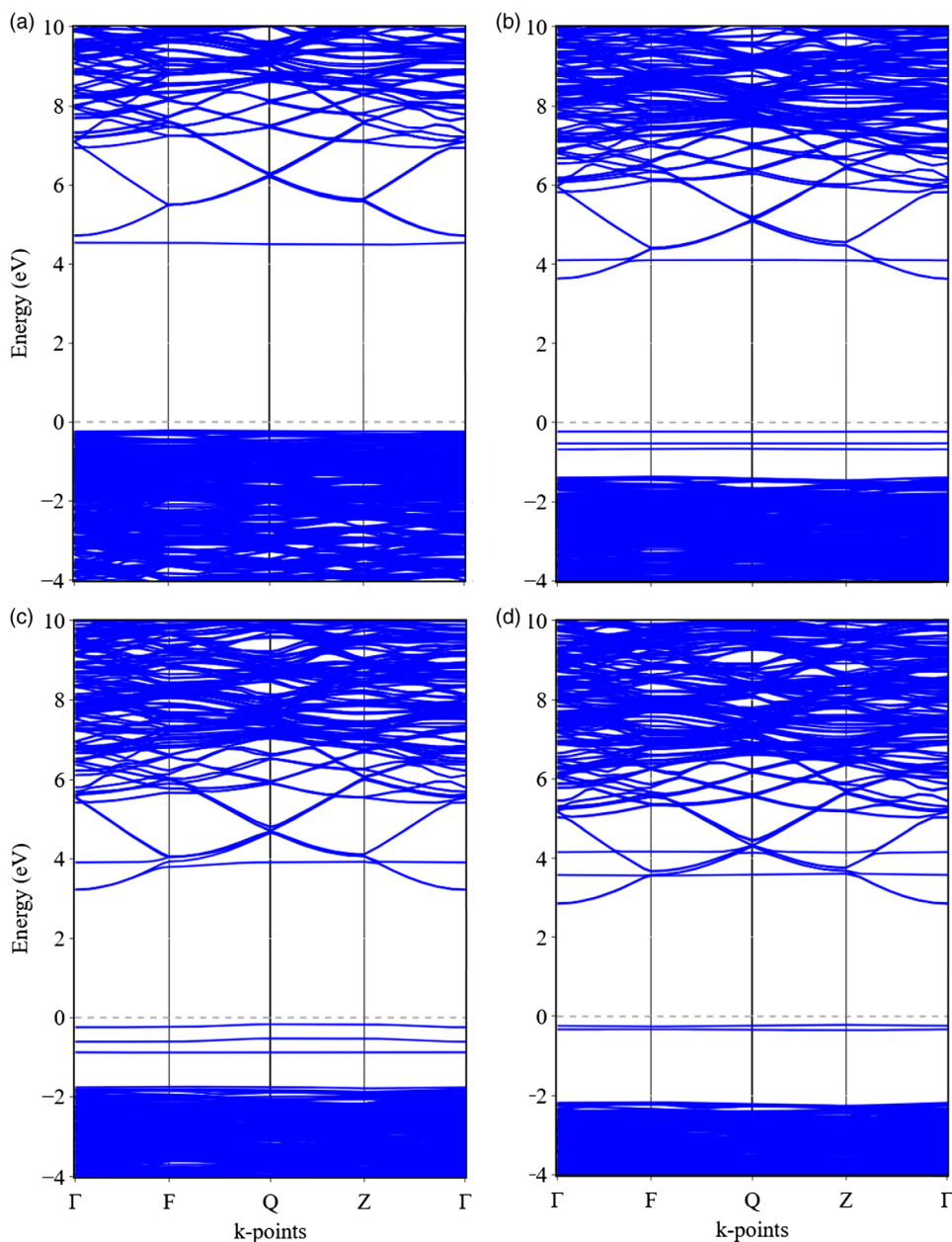


**Figure 6.** Band structure of  $\beta$ - $Ga_2O_3$  for the cases with defects/complexes for 0 charge state: a)  $N_{O_{II}}$ , b)  $N_{i8}$ , c)  $N_{i9}$ , and d)  $N_{i9}$ - $N_{O_I}$ .

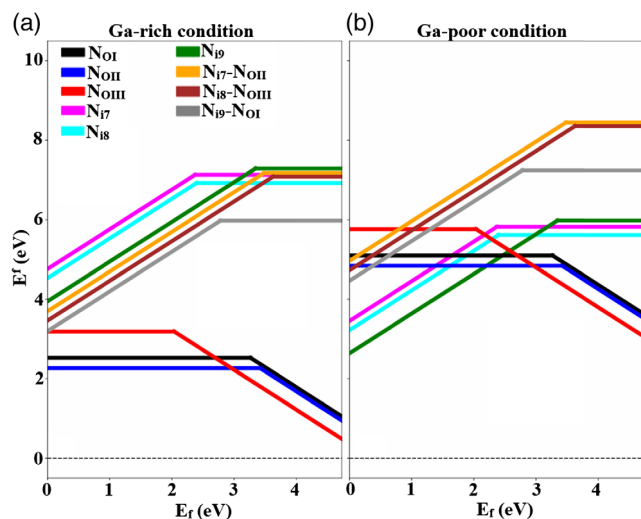


**Figure 7.** Calculated formation energy  $E_f^f$  for nitrogen defects/complexes in  $\beta$ - $\text{Ga}_2\text{O}_3$  as a function of Fermi energy  $E_f$  under a) Ga-rich and b) Ga-poor growth conditions. Note that  $E_f = 0$  eV corresponds to the valence band maximum (VBM), and  $E_f = 4.91$  eV corresponds to the conduction band minimum. Also note that the 2N-i7 case is not shown here as it has the highest formation energy among all examined defects.

**Table 2.** Transition levels for N-doped  $\beta$ - $\text{Ga}_2\text{O}_3$  for defects presented in Figure 7.

Defect	$\varepsilon(q_1/q_2)$	
	+1/0	0/-1
i7	2.54	–
i8	2.53	–
i9	3.44	–
$\text{N}_{i7}\text{-N}_{\text{OII}}$	3.73	–
$\text{N}_{i8}\text{-N}_{\text{OIII}}$	3.64	–
$\text{N}_{i9}\text{-N}_{\text{OI}}$	3.29	–
$\text{N}_{\text{OI}}$	–	3.44
$\text{N}_{\text{OII}}$	–	3.59
$\text{N}_{\text{OIII}}$	–	2.16

conditions, the formation energies of  $\text{N}_{i7}\text{-N}_{\text{OII}}$ ,  $\text{N}_{i8}\text{-N}_{\text{OIII}}$ , and  $\text{N}_{i9}\text{-N}_{\text{OI}}$  are comparable with the formation energies of the cases with the interstitial defects only, i.e., the  $\text{N}_{i7}$ ,  $\text{N}_{i8}$ , and  $\text{N}_{i9}$  cases. As in the case of the interstitial defects,  $\text{N}_{i7}\text{-N}_{\text{OII}}$ ,  $\text{N}_{i8}\text{-N}_{\text{OIII}}$ , and  $\text{N}_{i9}\text{-N}_{\text{OI}}$  are also deep acceptors. **Table 2** summarizes the transition levels for defects discussed in Figure 7 and confirms the deep nature of all donors and acceptors.

## 4. Conclusion

In summary, a comprehensive investigation of nitrogen defects in the low-symmetric monoclinic phase of  $\text{Ga}_2\text{O}_3$  using DFT with the HSE06 hybrid functional was conducted. Our study aimed also to assess the possibility of forming nitrogen  $\text{N}_2$ -like

complexes in  $\beta$ - $\text{Ga}_2\text{O}_3$ . In total, 3 substitutional and 11 distinct interstitial positions for the N atom were considered. Analysis of the formation energies allowed us to limit the number of interstitial defects for further computations to three:  $\text{N}_{i7}$ ,  $\text{N}_{i8}$ , and  $\text{N}_{i9}$ . These structures were used to produce four  $\text{N}_2$ -like complexes: three comprising one interstitial nitrogen and one nitrogen atom on an oxygen site ( $\text{N}_{i7}\text{-N}_{\text{OII}}$ ,  $\text{N}_{i8}\text{-N}_{\text{OIII}}$ , and  $\text{N}_{i9}\text{-N}_{\text{OI}}$ ) and one complex with both nitrogen atoms placed on i7 equivalent positions (2N-i7).

The calculations revealed that substitutional nitrogen defects act as deep acceptors, whereas the interstitial defects and  $\text{N}_2$ -like complexes act as deep donors. Under Ga-rich growth conditions, substitutional nitrogen defects exhibit lower formation energies, whereas, under Ga-poor conditions, interstitials  $\text{N}_{i7}$ ,  $\text{N}_{i8}$ , and  $\text{N}_{i9}$  show lower formation energies for a certain Fermi energy range. Notably, the formation of the  $\text{N}_2$ -like complex 2N-i7 is energetically very expensive regardless of growth conditions, consistent with similar studies of  $\text{N}_2$  in  $\beta$ - $\text{Ga}_2\text{O}_3$ <sup>[20]</sup> and  $\text{ZnO}$ <sup>[24]</sup> matrixes. Our results indicate that the considered interstitial defects and complexes also introduce stable spin-polarized states in  $\beta$ - $\text{Ga}_2\text{O}_3$ .

Overall, these findings provide valuable insights into the behavior of nitrogen as both a substitutional and interstitial defect, as well as its potential to form  $\text{N}_2$ -like complexes within the  $\beta$ - $\text{Ga}_2\text{O}_3$  matrix. This understanding is crucial for optimizing doping strategies and improving the performance of  $\beta$ - $\text{Ga}_2\text{O}_3$ -based electronic devices.

## Acknowledgements

This research was carried out with the support of the Interdisciplinary Center for Mathematical and Computational Modeling University of Warsaw (ICM UW) under computational allocation no. G35-57. The authors gratefully acknowledge Poland's high-performance Infrastructure PLGrid (HPC Centers: ACK Cyfronet AGH, PCSS, CI TASK, WCSS) for providing computer facilities and support within computational grant no. PLG/2023/016578. These studies were financially supported by the project UMO-2020/39/B/ST5/03580 founded by the National Science Centre (NCN) in Poland.

## Conflict of Interest

The authors declare no conflict of interest.

## Data Availability Statement

The data that support the findings of this study are available from the corresponding author upon reasonable request.

## Keywords

$\beta$ - $\text{Ga}_2\text{O}_3$ , electronic properties, hybrid-density-functional theories, interstitial defects, N dopants

Received: August 30, 2024  
Revised: September 11, 2024  
Published online:



- [1] D. C. Look, K. D. Leedy, *Sci. Rep.* **2019**, 9, 1290.
- [2] J. Zhang, J. Shi, D.-C. Qi, L. Chen, K. H. L. Zhang, *APL Mater.* **2020**, 8, 020906.
- [3] B. J. Baliga, *IEEE Electron Device Lett.* **1989**, 10, 455.
- [4] M. Higashiwaki, K. Sasaki, H. Murakami, Y. Kumagai, A. Koukitu, A. Kuramata, T. Masui, S. Yamakoshi, *Semicond. Sci. Technol.* **2016**, 31, 034001.
- [5] M. A. Mastro, A. Kuramata, J. Calkins, J. Kim, F. Ren, S. J. Pearton, *ECS J. Solid State Sci. Technol.* **2017**, 6, P356.
- [6] N. Moser, J. McCandless, A. Crespo, K. Leedy, A. Green, A. Neal, S. Mou, E. Ahmadi, J. Speck, K. Chabak, N. Peixoto, G. Jessen, *IEEE Electron Device Lett.* **2017**, 38, 775.
- [7] "Chapter 3 - Progress in semiconductor  $\beta$ -Ga $2$ O $3$ " in *Ultra-Wide Bandgap Semiconductor Materials - Materials Today* (Eds: M. Liao, B. Shen, Z. Wang), Elsevier, Amsterdam, Netherlands **2019**, pp. 263–345.
- [8] M. Baldini, Z. Galazka, G. Wagner, *Mater. Sci. Semicond. Process.* **2018**, 78, 132.
- [9] M. H. Wong, K. Goto, H. Murakami, Y. Kumagai, M. Higashiwaki, *IEEE Electron Device Lett.* **2018**, 40, 431.
- [10] M. Higashiwaki, K. Sasaki, A. Kuramata, T. Masui, S. Yamakoshi, *Appl. Phys. Lett.* **2012**, 100, 013504.
- [11] M. H. Wong, C.-H. Lin, A. Kuramata, S. Yamakoshi, H. Murakami, Y. Kumagai, M. Higashiwaki, *Appl. Phys. Lett.* **2018**, 113, 102103.
- [12] D. Gogova, M. Schmidbauer, A. Kwasniewski, *CrystEngComm* **2015**, 17, 6744.
- [13] S. Krishnamoorthy, Z. Xia, S. Bajaj, M. Brenner, S. Rajan, *Appl. Phys. Express* **2017**, 10, 051102.
- [14] E. Ahmadi, O. S. Koksaldi, S. W. Kaun, Y. Oshima, D. B. Short, U. K. Mishra, J. S. Speck, *Appl. Phys. Express* **2017**, 10, 041102.
- [15] J. L. Lyons, *Semicond. Sci. Technol.* **2018**, 33, 05LT02.
- [16] J. R. Ritter, J. Huso, P. T. Dickens, J. B. Varley, K. G. Lynn, M. D. McCluskey, *Appl. Phys. Lett.* **2018**, 113, 052101.
- [17] T. Zacherle, P. C. Schmidt, M. Martin, *Phys. Rev. B* **2013**, 87, 235206.
- [18] A. Kyrtsos, M. Matsubara, E. Bellotti, *Phys. Rev. B* **2017**, 95, 245202.
- [19] M. E. Ingebrigtsen, A. Y. Kuznetsov, B. G. Svensson, G. Alfieri, A. Mihaila, U. Badstübner, A. Perron, L. Vines, J. B. Varley, *APL Mater.* **2019**, 7, 022510.
- [20] H. Peelaers, J. L. Lyons, J. B. Varley, C. G. Van de Walle, *APL Mater.* **2019**, 7, 022519.
- [21] C. Ma, Z. Wu, H. Zhang, H. Zhu, J. Kang, J. Chu, Z. Fang, *Phys. Chem. Chem. Phys.* **2023**, 25, 13766.
- [22] W.-Z. Xiao, L.-L. Wang, L. Xu, Q. Wan, A.-L. Pan, *Solid State Commun.* **2010**, 150, 852.
- [23] N. H. Nickel, M. A. Gluba, *Phys. Rev. Lett.* **2009**, 103, 145501.
- [24] J. Gao, R. Qin, G. Luo, J. Lu, Y. Leprince-Wang, H. Ye, Z. Liao, Q. Zhao, D. Yu, *Phys. Lett. A* **2010**, 374, 3546.
- [25] Y. Kato, M. Yamamoto, A. Ozawa, Y. Kawaguchi, A. Miyoshi, T. Oshima, K. Maeda, T. Yoshida, *E-J. Surf. Sci. Nanotechnol.* **2018**, 16, 262.
- [26] M. A. Blanco, M. B. Sahariah, H. Jiang, A. Costales, R. Pandey, *Phys. Rev. B* **2005**, 72, 184103.
- [27] A. Shokri, Y. Melikhov, Y. Syryanny, I. N. Demchenko, *ACS Omega* **2023**, 8, 43732.
- [28] G. Kresse, J. Hafner, *Phys. Rev. B* **1994**, 49, 14251.
- [29] G. Kresse, J. Furthmüller, *Comput. Mater. Sci.* **1996**, 6, 15.
- [30] G. Kresse, J. Furthmüller, *Phys. Rev. B* **1996**, 54, 11169.
- [31] G. Kresse, D. Joubert, *Phys. Rev. B* **1999**, 59, 1758.
- [32] J. Heyd, G. E. Scuseria, M. Ernzerhof, *J. Chem. Phys.* **2003**, 118, 8207.
- [33] C. Freysoldt, J. Neugebauer, C. G. Van de Walle, *Phys. Rev. Lett.* **2009**, 102, 016402.
- [34] M. Passlack, N. E. J. Hunt, E. F. Schubert, G. J. Zyzdik, M. Hong, J. P. Mannaerts, R. L. Opila, R. J. Fischer, *Appl. Phys. Lett.* **1994**, 64, 2715.
- [35] A. Kyrtsos, M. Matsubara, E. Bellotti, *Appl. Phys. Lett.* **2018**, 112, 032108.
- [36] H. Peelaers, C. G. Van de Walle, *Phys. Status Solidi B* **2015**, 252, 828.
- [37] M. Mohamed, C. Janowitz, I. Unger, R. Manzke, Z. Galazka, R. Uecker, R. Fornari, J. R. Weber, J. B. Varley, C. G. Van de Walle, *Appl. Phys. Lett.* **2010**, 97, 211903.
- [38] T. Onuma, S. Saito, K. Sasaki, T. Masui, T. Yamaguchi, T. Honda, M. Higashiwaki, *Jpn. J. Appl. Phys.* **2015**, 54, 112601.
- [39] H. Peelaers, C. G. Van de Walle, *Appl. Phys. Lett.* **2017**, 111, 182104.
- [40] J. E. House, K. A. House, in *Descriptive Inorganic Chemistry*, Academic Press, Cambridge, MA **2015**, pp. 197–213.
- [41] L. K. Ping, M. A. Mohamed, A. K. Mondal, M. F. M. Taib, M. H. Samat, D. D. Berhanuddin, P. S. Menon, R. Bahru, *Micromachines* **2021**, 12, 348.